Environmental Science
Water Research & Technology

Impacts of Antiscalants on the Formation of Calcium Solids: Implication on Scaling Potential of Desalination Concentrate

Journal:	*Environmental Science: Water Research & Technology*
Manuscript ID	EW-ART-04-2019-000351
Article Type:	Paper
Date Submitted by the Author:	29-Apr-2019
Complete List of Authors:	Jain, Tushar; University of California, Riverside, Chemical and Environmental Engineering Sanchez, Edgar; University of California Riverside Owens-Bennett, Emily ; Trussell Technologies Inc Trussell, R.; Trussell Technologies, Walker, Sharon; University of California, Riverside, Chemical and Environmental Engineering Liu, Haizhou; University of California, Riverside, Chemical and Environmental Engineering

Water Impact Statement

The management of desalination brine has become increasingly important and a costly issue, especially in inland areas. In particular, the presence of oversaturated calcium as scale-forming compounds in the brine is challenging to dispose. I nthis study, we established a quantitative relationship to predict the nucleation rate of three commonly observed scale-forming calcium minerals in desalination brine and three widely used antiscalants. The modeling of precipitation rate from this study provided crucial information on the relationship among the rate of precipitation, antiscalant dosage and critical saturation index in desalination concentrate.

Impacts of Antiscalants on the Formation of Calcium Solids: Implication on Scaling Potential of Desalination Concentrate

Tushar Jain[†], Edgar Sanchez[†], Emily Owens-Bennett[‡],
Rhodes Trussell[‡], Sharon Walker[†] and Haizhou Liu[*†]

† Department of Chemical and Environmental Engineering, University of California at Riverside, Riverside, CA, 92521 USA

‡ Trussell Technologies, Inc. Pasadena, CA, 91101 USA

* Corresponding author, e-mail: haizhou@engr.ucr.edu, phone (951) 827-2076, fax (951) 827-5696.

Submitted to Environmental Science: Water Research & Technology

Abstract

Brackish water desalination has become increasingly important in arid inland regions for reliable water supplies, but the management of desalination brine waste is costly. In particular, the presence of oversaturated calcium as scale-forming compounds in the brine is challenging to disposal. This study investigated the effects of three widely used antiscalants, *i.e.,* nitrilotri-methylenephosphonic acid (NTMP), ethylenediaminetetra-methylenephosphonic acid (EDTMP) and diethylenetriaminepentakis-methylphosphonic acid (DTPMP) on the precipitation of calcium from solutions under chemical conditions relevant to brackish desalination brine, with an emphasis on the nucleation and precipitation of three calcium-containing solids including hydroxyapatite $Ca_5(PO_4)_3OH_{(s)}$, gypsum $CaSO_{4(s)}$, and vaterite $CaCO_{3(s)}$. The nucleation rates and activation energy of nucleation were investigated for the first time for hydroxyapatite relevant to a desalination concentrate. Results showed that all three antiscalants exhibited uniquely time-dependent effects on the inhibition of calcium solid formation. The precipitation kinetics exhibited a three-phase behavior, with an induction phase, a rapid reaction phase, and a final equilibrium phase. The effectiveness of antiscalant in delaying calcium precipitation and slowing down the rate of precipitation followed the order of DTPMP > EDTMP > NTMP. Antiscalants adsorb on the nuclei of calcium solids and inhibit the crystal growth process. Activation energy of nucleation increased linearly with antiscalant dosage, but it decreased as the regime changed from homogeneous to heterogeneous nucleation. This study generated vital information on the precipitation kinetics of calcium solids in the presence of phosphonate-containing antiscalants and advances the development of desalination brine management strategies.

Introduction

As freshwater scarcity becomes more severe with increasing population and climate change impacts, alternative water sources - in particular, brackish groundwater - have become increasingly important for arid inland regions.[1,2] Brackish groundwater is usually formed as a result of geological salt deposition or long-term agricultural activities.[3-5] It typically contains total dissolved solids (TDS) levels between 1 and 10 g/L.[6-8] In recent years, membrane-based brackish water desalination has been increasingly implemented to supply drinking water in inland areas worldwide, including Australia, the Middle East and the United States.[9-13] For example, the operational and planned brackish groundwater desalination plants in California have a combined annual capacity of 260 million gallons per day as of 2013.[14]

Another major challenge with desalination is scaling of the membranes themselves, a phenomenon attributed to the inevitable precipitation of calcium-containing minerals including calcium sulfate $CaSO_{4(s)}$, calcium carbonate $CaCO_{3(s)}$ and calcium phosphate $Ca_5(PO_4)_3OH_{(s)}$ at the membrane surface.[15,16] The efficiency of reverse osmosis based brackish water desalination is inherently limited by membrane scaling. To control membrane scaling, scale-inhibiting chemicals known as antiscalants are added to the feed water.[17-19] These chemicals interfere with the nucleation process of calcium solids and retard the crystal growth.[20] The continuous application of antiscalants in the feed water results in an oversaturation of dissolved calcium that coexists with antiscalants in the brackish desalination concentrate (also known as brine).[21,22] Meanwhile, the inhibiting effects of antiscalants on the precipitation of calcium solids are time sensitive. For example, in the Inland Empire of Southern California, a 70-mile brine pipeline system

carries inland brackish water desalination concentrate to a coastal disposal facility.[23] The presence of antiscalants in the discharged brine prevents calcium precipitation at the entry points along the brine line, but as the brine wastewater travels along the pipeline, a substantial amount of additional solids are generated, creating problematic scaling issues in the pipeline.[24,25] Other studies similarly reported the delayed precipitation of solids in membrane concentrate.[26-28] This inadvertent solid formation and associated challenge with scale formation during brine disposal make it urgent to understand the effects of antiscalants on solid formation.

Furthermore, recovery of water from desalination brine is important to minimize brine disposal cost. However, the presence of oversaturated scale-forming calcium in the brine is undesirable to additional water recovery. In contrast, a tunable control on antiscalants can potentially accelerate the precipitation of calcium solids. This decrease in scale-forming constituents can help achieve higher recovery of water from brine using secondary membrane units. Therefore, it is critical to understand the nature and effects of antiscalants on the chemical stability of calcium solids in the brine, which can lead to the development of sustainable concentrate management for inland desalination.

Most antiscalants are organic phosphorus chemicals known as phosphonic acids. They contain multiple phosphonate functional groups ($-PO_3H_2$) within a tertiary amine structure.[29,30] The phosphorus-carbon bond in antiscalants exhibits a good thermal stability,[31] and promotes their applications in desalination plants as well as cooling towers.[32,33] The concentration of phosphonic acids in desalination processes depend on the composition of the feedwater. For brackish water desalination concentrate it is typically in the range of 2-10 μM.[34,35] In particular, nitrilotri-methylenephosphonic acid (NTMP),

ethylenediaminetetra-methylenephosphonic acid (EDTMP) and diethylenetriaminepentakis-methylphosphonic acid (DTPMP) are among the most widely used antiscalants in water industry.[36-39] Their molecular structures are shown in Figure S1 of the SI section.

Prior studies examined the impact of different antiscalants on the precipitation of calcite, gypsum, silica, *etc*.[29,40-42] Multiple studies have tried to quantify the dose response of antiscalants with respect to the extent of supersaturation.[19,43,44] Recent studies investigated the cost associated with maximizing the water recovery in membrane desalination process for brackish water with these scaling minerals.[45] Phosphonic antiscalants can also form complexes with calcium and undergo multiple steps of deprotonation.[46-48] However, the effect of antiscalants on the nucleation and crystal growth process of calcium solids remains unknown. Typically, the onset of solid precipitation is delayed in the presence of antiscalants. This delayed period, known as induction time, is controlled by the activation energy of the nucleation process.[49,50] A better and quantitative understanding on how antiscalants impact the induction time is critical to predict the effectiveness of antiscalants. Furthermore, although the presence of antiscalants delays nucleation reaction, the nuclei formation eventually takes place. Therefore, it is important to quantify the kinetics of solid precipitation in the presence of antiscalants.

In recent years, membrane-based advanced reuse of domestic wastewater in agricultural and industrial sectors have been increasingly implemented. Reclaimed wastewater is also increasingly used for industry and landscaping. Sparingly soluble hydroxyapatite $Ca_5(PO_4)_3OH_{(s)}$ in the brine becomes a major limiting factor in these scenarios where the reclaimed water is rich in phosphate.[51-54] While there are studies mainly focused on the

commonly observed scaling minerals such as $CaSO_{4(s)}$ and $CaCO_{3(s)}$,[55-58] To the our best of knowledge, no study has looked into the impact of antiscalants on the precipitation mechanisms and kinetics of hydroxyapatite nucleation. However, the nature of calcium phosphate formation and the associated antiscalant effect remains to be understood.

The objectives of this study were to examine the impacts of three widely used antiscalants (*i.e.*, NTMP, EDTMP and DTPMP) in brackish water concentrate on the nucleation process of calcium-containing solids (*i.e.*, $Ca_5(PO_4)_3OH_{(s)}$, $CaSO_{4(s)}$, and $CaCO_{3(s)}$), quantify the precipitation kinetics of calcium solid formation, and the nature of calcium phosphate nucleation in presence of these antiscalants.

Materials and methods

The solution chemical matrix for the precipitation experiments was selected based on the chemical composition of the brackish RO concentrate. A synthetic concentrate allowed us to precisely control and vary the saturation indices of different calcium minerals. This simplified setup also helped us to understand the fundamentals of nucleation of different calcium minerals in presence of the antiscalants. All solutions were prepared with analytical grade chemicals and deionized (DI) water (resistivity < 18.2 MΩ/cm). To start a precipitation experiment with $Ca_5(PO_4)_3OH_{(s)}$, stock solutions of 25-50 mM $CaCl_2$ and 1-3 mM Na_2HPO_4 were prepared and adjusted to pH 7.8 with droplets of 0.5 M NaOH and 0.5 M $HClO_4$ at a temperature of 20 °C. This pH level is typical of brackish water desalination brine.[59] Initial ionic strength of the mixing solution was fixed at 0.1 M by adding targeted amount of $NaClO_4$.

A 150 mL solution containing $CaCl_2$ and a 100 mL solution containing Na_2HPO_4 were adjusted to pH 7.8. Following that, 0-10 mM of NTMP, EDTMP or DTPMP prepared from its respective sodium-based salt was added into $CaCl_2$ and Na_2HPO_4 solutions with equal concentrations. Both solutions were then quickly mixed at a high stirring rate in a batch reactor at 20 °C. This approach of mixing avoided possible interference due to localized concentration spikes. The final mixed solution created a targeted antiscalant concentration typical to a brackish water desalination brine, ranging between 0 and 11 μM, and a saturation index between 14 and 15 with respect to $Ca_5(PO_4)_3OH_{(s)}$. The saturation index of $Ca_5(PO_4)_3OH_{(s)}$ is defined as:

$$SI_{Ca_5(PO_4)_3OH} = \log\left(\frac{\alpha_{Ca^{2+}}^5 \times \alpha_{PO_4^{3-}}^3 \times \alpha_{OH^-}}{K_{sp,\ Ca_5(PO_4)_3OH_{(s)}}}\right) \quad (1)$$

where $\alpha_{PO_4^{3-}}$, α_{OH^-} and, $\alpha_{Ca^{2+}}$ are activities of PO_4^{3-}, OH^- and Ca^{2+}, respectively. $K_{sp,\ Ca_5(PO_4)_3OH_{(s)}}$ is the solubility product of hydroxyapatite ($10^{-44.33}$). Equilibrium calculations and stability constants were from the Visual MINTEQ software database.[60]

The precipitation experiments with $CaSO_{4(s)}$ and $CaCO_{3(s)}$ were performed similarly to that of $Ca_5(PO_4)_3(OH)_{(s)}$, except that phosphate was replaced by sulfate and carbonate salt, respectively. The saturation index was controlled between 0.2 to 1.2 for $CaSO_{4(s)}$. The saturation index for $CaCO_{3(s)}$ was varied between 1.3 and 1.8 by adjusting the alkalinity from 10 to 36 mM as carbonate. The saturation index of each solid is defined as:

$$SI_{CaSO_4} = \log\left(\frac{\alpha_{Ca^{2+}} \times \alpha_{SO_4^{2-}}}{K_{sp,\ CaSO_{4(s)}}}\right) \quad (2)$$

$$SI_{CaCO_3} = \log\left(\frac{\alpha_{Ca^{2+}} \times \alpha_{CO_3^{2-}}}{K_{sp,\ CaCO_{3(s)}}}\right) \quad (3)$$

Where $\alpha_{SO_4^{2-}}$, $\alpha_{CO_3^{2-}}$ and $\alpha_{Ca^{2+}}$ are the activities of SO_4^{2-}, CO_3^{2-} and Ca^{2+}, respectively, while $K_{sp,\ CaSO_4}$ and $K_{sp,\ CaCO_3}$ are the solubility products of calcium sulfate and calcium carbonate, respectively ($K_{sp,\ CaSO_4} = 10^{-4.61}$, $K_{sp,\ CaCO_3} = 10^{-8.48}$).[61]

After the mixing of respective solutions, precipitation experiments were conducted in a 250 mL batch reactor completely mixed at 400 rpm with a magnetic stir bar. The solid precipitation kinetics were monitored by measuring the change of turbidity at pre-determined time intervals using a HACH 2100N turbidimeter. The suspension pH was maintained at 7.8 ± 0.05 with a requisite amount of tris(hydroxymethyl)aminomethane (TRIS) buffer. The presence of TRIS buffer has a negligible impact on the calcium precipitation reaction (Figure S2). The rate of precipitation was calculated by fitting the turbidity-time profile to a Michaelis-Menten type model.[62] The rate model and the fitting are described in Text S1 and Figure S3. The concentration of antiscalants was confirmed by UV oxidation with H_2O_2 followed by analysis of phosphate using the standard molybdate blue spectrophotometric method.[63] Zeta potential of precipitated calcium solids was measured using Zetasizer nano ZS90 analyzer (Malvern Panalytical, Inc.). The mineral phases of precipitated solids were analyzed by X-ray diffraction (XRD) and three calcium solids were confirmed (Figure S4).

Results and discussions

Effect of antiscalant type on the precipitation of calcium solids

Figure 1A shows the kinetics of hydroxyapatite precipitation reactions in the presence of three antiscalants. The precipitation kinetics on the basis of the solution turbidity exhibited three distinct phases: an initial lag phase, a rapid precipitation phase and a final equilibrium phase. During the lag stage, hydroxyapatite nuclei underwent a constant formation and dissolution until a critical radius (denoted as $r_{critical}$) was achieved. This initial phase was followed by a rapid precipitation phase where crystals grew quickly until reaching equilibrium and becoming stationary in the end.

In the presence of 1 μM NTMP, EDTMP or DTPMP, the induction time for hydroxyapatite precipitation to occur ranged between 1 and 5 minutes (Figure 1A). Phosphonate antiscalants can adsorb onto the incipient nuclei generated during the induction period, resulting in a distortion of crystal growth pattern and a delay of nucleation.[64-66] Antiscalants can also act as an impurity on the surface of a growing crystal, which slows down its further growth. The presence of antiscalants can increase the surface energy of the growing crystals, which decreases the rate of nucleation and increases the induction time.[67]

The induction time of hydroxyapatite precipitation without an antiscalant was only a few seconds. It significantly increased in the presence of an antiscalant compared to the control (Figure 1A). Calculations showed that a majority of calcium under the brine chemical condition exists as the free ion form rather than aqueous calcium-antiscalant complexes in the presence of antiscalants (Text S2 and Figure S5), indicating that the inhibitive effect by antiscalants likely results from the adsorption of antiscalants onto the incipient nuclei of hydroxyapatite.

In addition, the effectiveness of antiscalant in extending the induction time followed the order of DTPMP > EDTMP > NTMP (solid lines in Figure 1B). The longer induction time

of hydroxyapatite nucleation in the presence of DTPMP compared to NTMP or EDTMP is likely contributed by two factors. First, antiscalants differ from each other in the number of amine functional groups in their backbone structure and the number of phosphonate groups (Figure S1). High-molecular-weight antiscalants with a larger number of amine groups (*e.g.*, DTPMP) have a bigger molecular structure compared to the relatively low-molecular-weight antiscalants (*e.g.*, NTMP). When antiscalants adsorb on the incipient hydroxyapatite nuclei, the high-molecular-weight DTPMP molecules occupy a larger surface area of the nuclei structure, thus extending the induction time considerably.[31,68]

Second, different antiscalants possess different surface charges. Calculations showed that DTPMP is the most negatively charged molecule among the three antiscalants (Text S3 and Figure S6). Meanwhile, the point of zero charge for hydroxyapatite in the brine solution was measured as 8.21 (Figure S7A), consistent with prior literature.[69,70] At pH 7.8, the surface of hydroxyapatite nuclei is positively charged and promotes the electrostatic adsorption of DTPMP. Consequently, it enhanced the effectiveness of DTPMP in delaying the induction time. Experimental data also confirmed that the surface charge of hydroxyapatite was reduced upon DTPMP adsorption (Figure S7B).

The mechanism of antiscalant inhibition on hydroxyapatite nucleation was further investigated by quantifying the steady-state nucleation rates, which is calculated as:

$$J_s = F \times \exp\left(\frac{-\beta\gamma_s^3 N_A f(\theta)}{(RT)^3 \mathrm{SI}^2}\right) \quad (4)$$

where F is the pre-exponential factor and has a theoretical value of 10^{33} nuclei·L^{-3}·s^{-1}, β is the shape factor ($16\pi/3$ for spherical nuclei), γ_s is the surface energy of crystallization

207 (J/m^2), N_A is the Avogadro's number (mol^{-1}), *f(θ)* is the correction factor (value=1 for
208 homogeneous nucleation),[58] *R* is the gas constant (8.3 $J \cdot mol^{-1} \cdot K^{-1}$), *T* is the absolute
209 temperature (K), and SI is the saturation index. Results showed that the nucleation rate
210 dropped with an increasing antiscalant dosage (dashed lines in Figure 1B). This trend is
211 also consistent with the extension of induction time (solid lines Figure 1B). A decrease in
212 the nucleation rate consequentially increases the time required for the crystal to grow and
213 delays the onset of precipitation.

214 Furthermore, with the same saturation index of hydroxyapatite, the induction time
215 increased with the antiscalant dosage (Figure 2A). For instance, an increase of EDTMP
216 dosage from 0.5 to 3 μM increased the duration of induction time from 1.5 to 5 minutes,
217 thus delaying the onset of homogeneous crystallization. A higher antiscalant concentration
218 in the solution resulted in a higher surface adsorption of the nuclei and less surface area
219 was available for the nucleation to take place. In addition, the effects of antiscalant on the
220 induction time also depends on the extent of calcium supersaturation. For example, a higher
221 saturation index of hydroxyapatite reduced the induction time at the same dosage of
222 EDTMP (Figure 2B).

223 Typically, as the dosage of antiscalant increased, it became more effective in delaying the
224 onset of hydroxyapatite precipitation with a more oversaturated solution, as shown by the
225 extension of induction time with an increasing antiscalant dosage at a fixed saturation index
226 (Figure 3). Furthermore, the three antiscalants exhibited different effectiveness in delaying
227 hydroxyapatite precipitation, which is evaluated based on the critical saturation index
228 (CSI). For a given antiscalant dosage, CSI is defined as the maximum saturation index
229 below which a decrease in the saturation index shows a significant increase in the induction

time. This was quantified by measuring the slope of induction time *vs*. the saturation index (Figure 3) and the CSI was the saturation index below which the average slope shows more than 40% change compared to its previous value. A higher CSI suggests a stronger inhibiting effect by antiscalant in precipitation. For example, at a dosage of 0.5 μM, NTMP only became effective in delaying hydroxyapatite precipitation at a saturation index less than 14.40 (Figure 3A), whereas EDTMP became effective with a saturation index less than 14.55 (Figure 3B), and DTPMP was effective when saturation index was below 14.69 (Figure 3C). A similar trend was also observed for $CaSO_{4(s)}$ and $CaCO_{3(s)}$ precipitation, respectively (Figure S8). These critical saturation indices are significant in defining the inhibitive effects of antiscalants on scale formation in desalination concentrate. These trends are also consistent with the observation that inhibition effects on calcium solids precipitation follow the order of DTPMP > EDTMP > NTMP.

Thermodynamics of calcium crystallization in the presence of antiscalants

According to the theory of homogenous nucleation, the duration of induction time is intrinsically associated with the thermodynamics of nucleation reaction and crystal growth process. Specifically, the logarithm of induction time is linearly related to the square root of the saturation index of the corresponding solid as described in the equation below:[71,72]

$$\log\left(t_{\mathrm{ind}}\right) = A\,T^{-3}(\mathrm{SI})^{-2} + B \qquad (5)$$

where t_{ind} is the induction time (second), T is the solution temperature (Kelvin), SI is the saturation index of the solution with respect to a calcium-containing solid (dimensionless), and both A and B are fitting parameters. This linear relationship was observed during the precipitation of $Ca_5(PO_4)_3OH_{(s)}$, $CaCO_{3(s)}$ and $CaSO_{4(s)}$ (Figure S9).

The surface energy of crystallization, γ_s (J/m^2), was calculated using the equation 6 below using the value of A obtained from equation 5:

$$\gamma_s = \left(\frac{A\,(2.3R)^3}{\beta V_m^2 N_A f(\theta)} \right)^{1/3} \quad (6)$$

where β is the geometry factor and has a value of $16\pi/3$ for a spherical nucleus, V_m is the molecular volume of the crystal (1.2×10^{-28} m^3/molecule for gypsum,[73] 6.1×10^{-29} m^3/molecule for vaterite,[74] and 2.6×10^{-28} m^3/molecule for hydroxyapatite[75,76]).

The Gibbs free energy of homogenous nucleation with respect to the radius of the nucleus is calculated as:[77-79]

$$\Delta G = -\frac{4\pi r^3 kT(\mathrm{SI})}{3V_m} + 4\pi r^2 \gamma \quad (7)$$

where k is the Boltzmann constant (1.38×10^{-23} J·K^{-1}). The first term in Equation 7 represents the change in the bulk free energy. The second term is the change in the surface free energy that results from the formation of new interface between the new nuclei and the aqueous phase.

When the Gibbs free energy of nucleation reaches a maximum, the radius of the nucleus is defined as the critical radius of nucleation ($r_{critical}$), and the corresponding Gibbs free energy is defined as the activation energy of nucleation ($\Delta G_{critical}$). $r_{critical}$ is the minimal radius of the nucleus that is required for the initiation of crystal growth and precipitation. A typical calculated trend of the nucleation process is shown in Figure 4A. For Equation 7, when r = $r_{critical}$, $(d\Delta G/dr) = 0$. Therefore,

$$r_{\text{critical}} = \frac{2\gamma V_{\text{m}}}{kT(\text{SI})} \quad (8)$$

Accordingly, a combination of Equations 7 and 8 results in the following expression:

$$\Delta G_{\text{critical}} = \frac{16\pi\gamma^3 {V_{\text{m}}}^2}{3\, k^2 T^2 \text{SI}^2} \quad (9)$$

Calculations show that values of $\Delta G_{\text{critical}}$ and r_{critical} decreased with an increase in saturation index (Figures S10-S11). A higher oversaturation level increases the probability of collisions between nuclei, and exerts a stronger driving force for nucleation, therefore decreasing the requirement on the size of subcritical nuclei reaching the r_{critical}.

To understand the effect of antiscalants on the precipitation thermodynamics, the effect of antiscalant dosage on the activation energy of calcium solid nucleation was investigated. Figure 4B shows a plot of relative changes in activation energy of nucleation ($\Delta G_{\text{critical}}$) as a function of EDTMP dosage for different calcium solids. $CaCO_{3(s)}$ and $CaSO_{4(s)}$ showed a linear increase in the activation energy with an increasing EDTMP dosage. $Ca_5(PO_4)_3OH_{(s)}$, however, only showed a similar trend at a low EDTMP dosage up to 1 μM, and its activation energy decreased with a further increase in the EDTMP dosage from 1 μM to 4 μM (open circles, Figure 4B).

The decrease in the activation energy of nucleation of $Ca_5(PO_4)_3OH_{(s)}$ at higher EDTMP dosages can be attributed to a transition from homogenous to heterogeneous nucleation. Plotting the log of induction time of hydroxyapatite in presence of EDTMP against the saturation ratio exhibited two distinct linear correlations (Figure S9A), suggesting a transition from homogenous to heterogenous nucleation when the saturation index

decrease. This effect was only observed with lower saturation indices and higher antiscalant dosages. Similar findings were reported for the precipitation of calcium solids changing from homogeneous to heterogenous nucleation at lower saturation indices.[72] The heterogeneous nucleation can take place due to the presence of freshly formed hydroxyapatite acting as seeds for nucleation.[80] The free energy barrier is smaller for heterogeneous nucleation compared to that for homogeneous nucleation.[81] Thus, to calculate the homogeneous activation energy of hydroxyapatite nucleation the results with higher antiscalant dosage and lower saturation indices conditions were discarded. The recalculated results showed a linear increase with EDTMP dosage (closed circles, Figure 4B).

Effect of antiscalant on the kinetics of calcium solids precipitation

The rate of hydroxyapatite precipitation depended on the antiscalant dosage and the saturation index (Figure 5). In general, at a fixed level of oversaturation, the rate of precipitation decreased with an increasing antiscalant dosage. Meanwhile, the rate of precipitation increased with a higher saturation index for any given antiscalant dosage.

In addition, different antiscalants exhibited distinct dosage-response behaviors on the precipitation rate. For example, NTMP showed a very strong dosage effect that highly depends on the level of oversaturation (Figure 5A). At a fixed NTMP dosage, as the saturation index increased beyond a critical value, the precipitation rate increased significantly. On the contrary, the dosage effect of EDTMP on the precipitation rate was moderate (Figure 5B), and that of DTPMP was insensitive to the saturation index (Figure 5C). The use of EDTMP or DTPMP at a low dosage of 0.5 μM is as effective as higher dosages in slowing down the precipitation kinetics regardless of calcium saturation, but

NTMP at 0.5 μM was only effective at a low calcium saturation level. These trends suggest that EDTMP and DTPMP are more effective than NTMP in suppressing the rate of hydroxyapatite precipitation. This difference likely resulted from a higher surface blockage of nuclei by the larger antiscalant molecules of EDTMP and DTPMP, and the consequently stronger inhibitive effects on the growth of calcium crystals.

Conclusion

These findings show that although all three of the antiscalants considered have active phosphonate functional groups, they affect the precipitation kinetics of calcium solids differently. Antiscalants are only effective in temporarily stabilizing the oversaturated desalination brine and delay the scale-forming substances (in this case, calcium solids) from precipitation. Results from this study established a quantitative relationship between the nucleation rate of three most commonly observed calcium-scaling solids and three most widely used antiscalants. Accordingly, it provided guidance on the threshold dosage of these antiscalants that can hold a certain duration of time to prevent the oversaturated brine waste from scale formation. Furthermore, with an ever-increasing dependence on desalination, especially in inland areas, and more desalination facilities targeting a near zero liquid discharge, brine demineralization (*i.e.*, TDS removal) is the key to increasing water recovery and managing the concentrate waste. The modeling of precipitation rates from this study provided crucial information on the relationships among the rate of precipitation, the antiscalant dosage, and the critical saturation index; together these can help to determine the targeted amount of antiscalant that needs to be removed to achieve a high rate of demineralization. The optimization of an efficient demineralization technique is crucial and will be further investigated in the future.

Acknowledgement

This research was supported by grants to H.L. from the National Science Foundation (Grant #1611306) and to T.J. from the National Water Research Institute. We thank the assistance of John Orta at UCR, Jesus Trujillo from San Bernardino Middle College High School and Osvaldo Mireles from San Bernardino Valley College on participation.

Supporting Information Section

Additional description of molecular structures of the antiscalants, calculation procedure for kinetic modeling, XRD spectra, free calcium ion calculations in each antiscalant system and antiscalant molecular charge calculations, figures on induction time and activation energy dependence on antiscalant concentration and saturation index are available in the SI section.

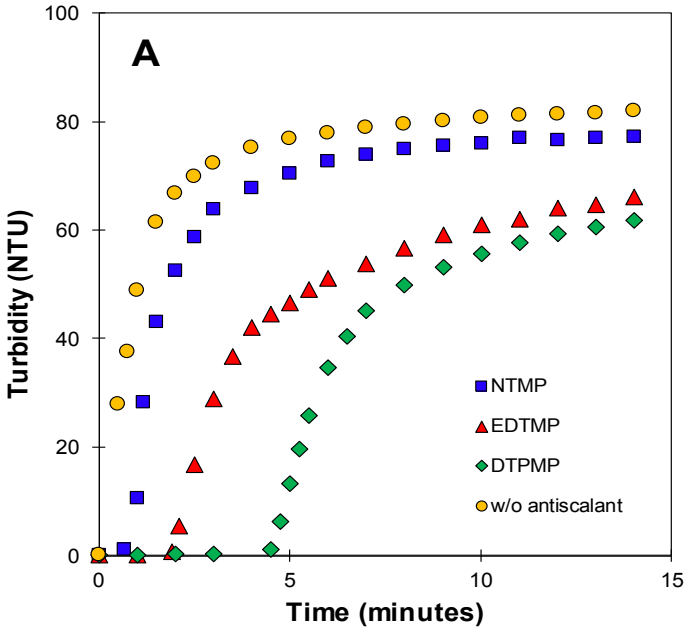

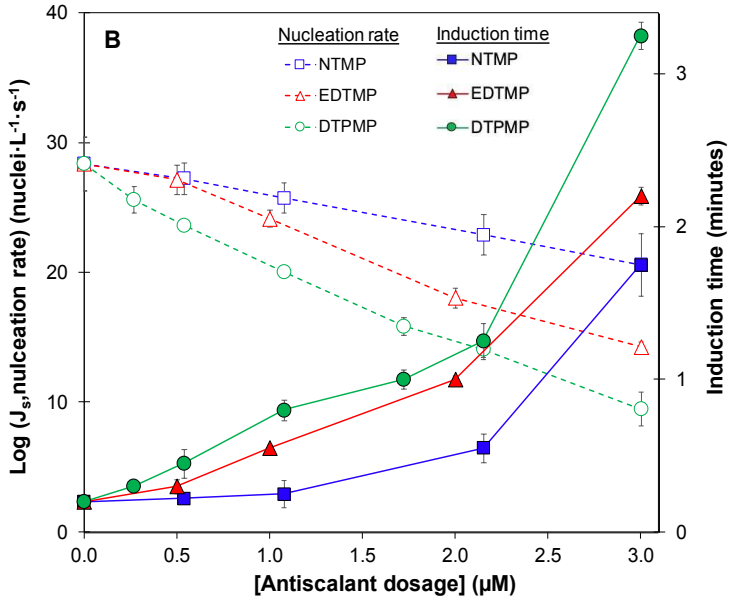

Figure 1 (A) Comparison among three antiscalants on their effects on the kinetics of hydroxyapatite precipitation. [Ca^{2+}] = 10 mM; [PO_4^{3-}] = 26 mg P/L; saturation index = 14.2; [antiscalant] = 1 μM. pH = 7.8; ionic strength = 100 mM; [TRIS buffer] = 20 mM. (B) Impact of different antiscalant dosage on the induction time (solid lines) and the nucleation rate (dashed lines) of hydroxyapatite. [Ca^{2+}] = 10 mM; [PO_4^{3-}] = 30 mg P/L; saturation index = 14.6; pH = 7.8; ionic strength = 100 mM; [TRIS buffer] = 20 mM.

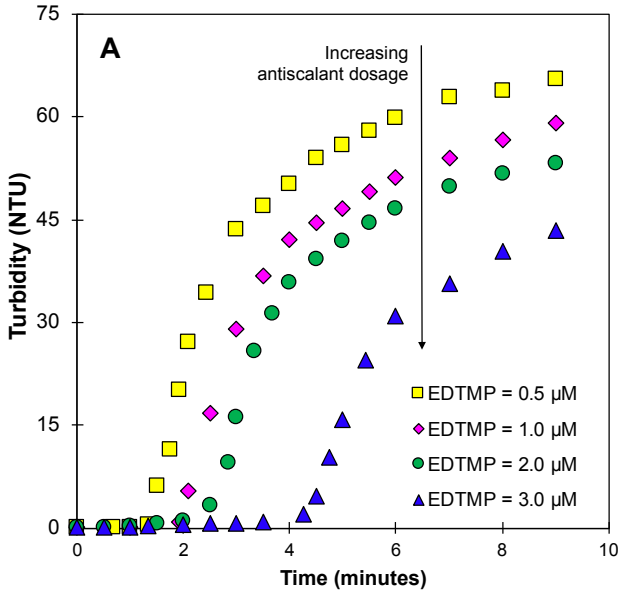

351

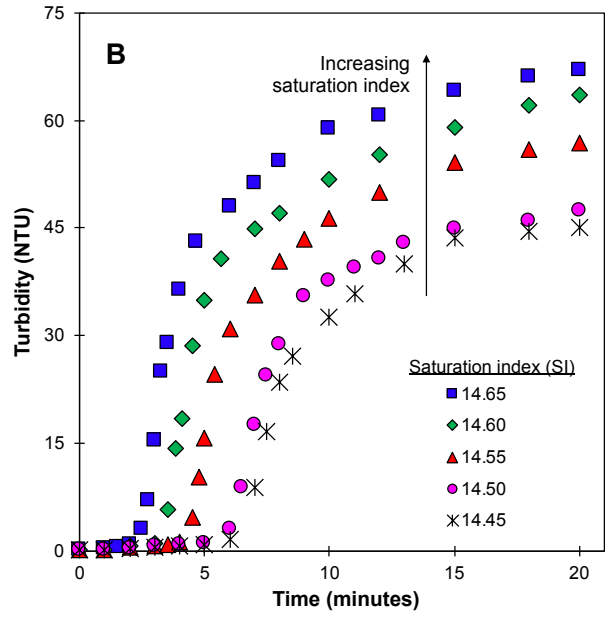

352

353 **Figure 2** The effects of EDTMP dosage and saturation index on induction time of

354 precipitation of hydroxyapatite. (A) $[Ca^{2+}]$ = 10 mM; $[PO_4^{3-}]$ = 26 mg P/L; saturation index

355 = 14.2; EDTMP = 0-3 µM; pH = 7.8; ionic strength = 100 mM; [TRIS buffer] = 20 mM.

356 (B) $[Ca^{2+}]$ = 10 mM; $[PO_4^{3-}]$ = 22-25 mg P/L; EDTMP = 2 µM; pH = 7.8; ionic strength =

357 100 mM; [TRIS buffer] = 20 mM.

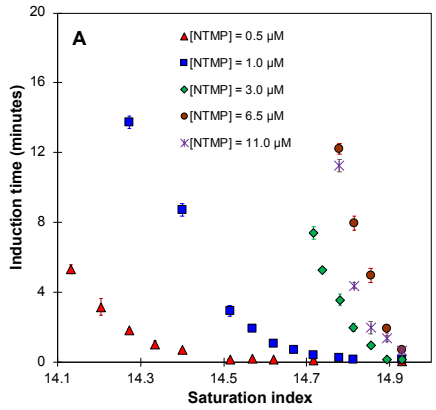

358

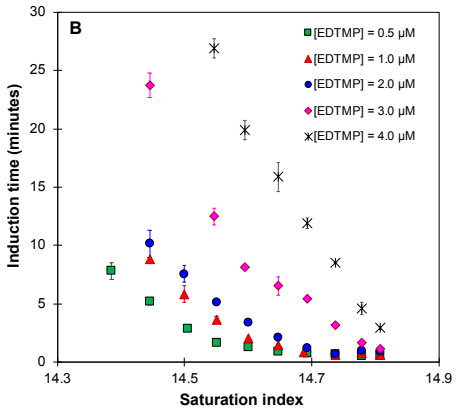

359

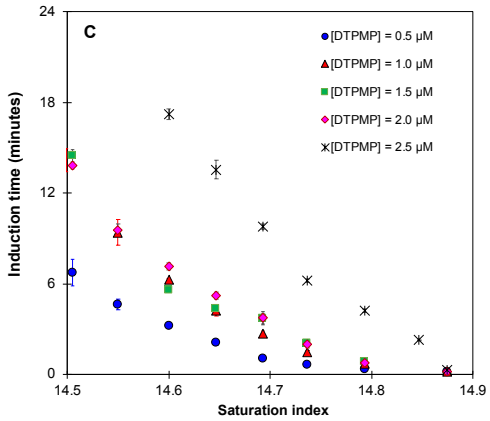

360 **Figure 3** The effect of antiscalant dosage on induction time of precipitation of
361 hydroxyapatite. (A) $[Ca^{2+}]$ = 10 mM; $[PO_4^{3-}]$ = 17-34 mg-P/L; saturation index = 14.1-
362 14.9; pH = 7.8; ionic strength = 100 mM; [TRIS buffer] = 20 mM. (B) $[Ca^{2+}]$ = 10 mM;
363 $[PO_4^{3-}]$ = 22-31 mg-P/L; saturation index = 14.3-14.8; pH = 7.8; ionic strength = 100 mM;
364 [TRIS buffer] = 20 mM. (C) $[Ca^{2+}]$ = 10 mM; $[PO_4^{3-}]$ = 24-35 mg P/L; saturation index =
365 14.5-14.9; pH = 7.8; ionic strength = 100 mM; [TRIS buffer] = 20 mM.

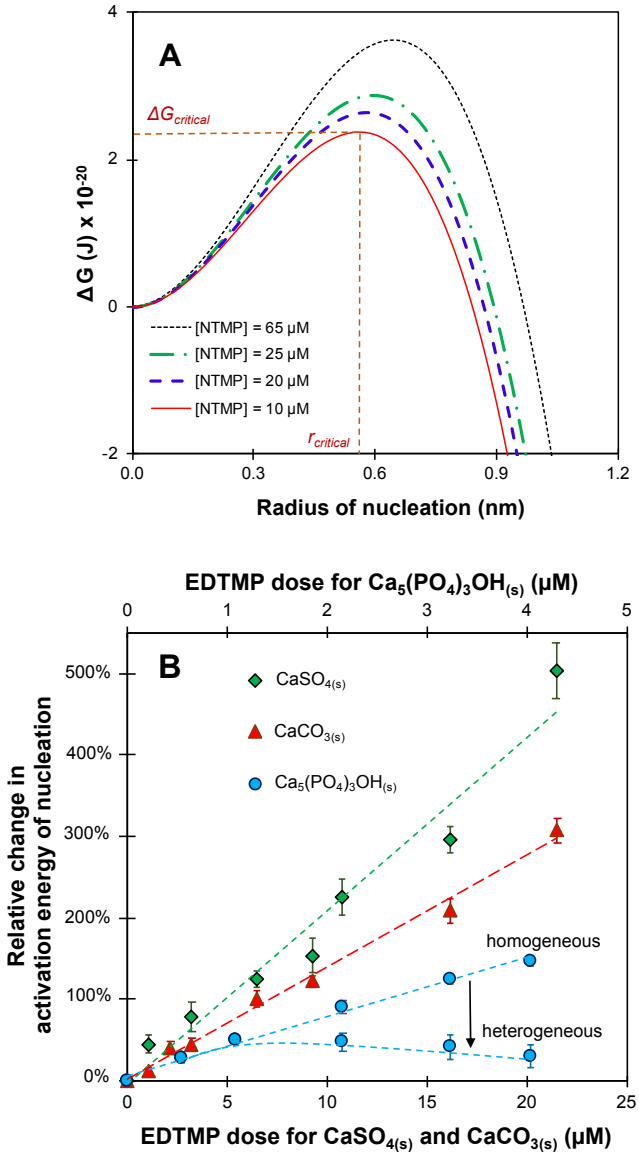

Figure 4 (A) Gibbs free energy for homogeneous nucleation of $CaSO_{4(s)}$ at varying NTMP dosages. $[Ca^{2+}] = 37$ mM; $[SO_4^{2-}] = 564$ mM; Saturation index = 0.84; pH = 7.8. (B) Impact of EDTMP dose on activation energy of different calcium solids; Experimental conditions for $CaCO_{3(s)}$: $[Ca^{2+}] = 10$ mM; $[CO_3^{2-}] = 10$ mM; [EDTMP] = 0-21 μM; saturation index = 1.32; pH = 7.8; ionic strength = 100 mM; [TRIS buffer] = 50 mM; Experimental conditions for $CaSO_{4(s)}$: $[Ca^{2+}] = 37$ mM; $[SO_4^{2-}] = 564$ mM; [EDTMP] = 0-21 μM; saturation index = 7; pH = 7.8; ionic strength = 1M. Experimental conditions for $Ca_5(PO_4)_3OH_{(s)}$: homogeneous nucleation (closed circles), heterogeneous nucleation (open circles); $[Ca^{2+}] = 10$ mM; $[PO_4^{3-}] = 0.6$ mM; [EDTMP] = 0-4 μM; saturation index = 14.2; pH = 7.8; ionic strength = 100 mM; [TRIS buffer] = 20 mM.

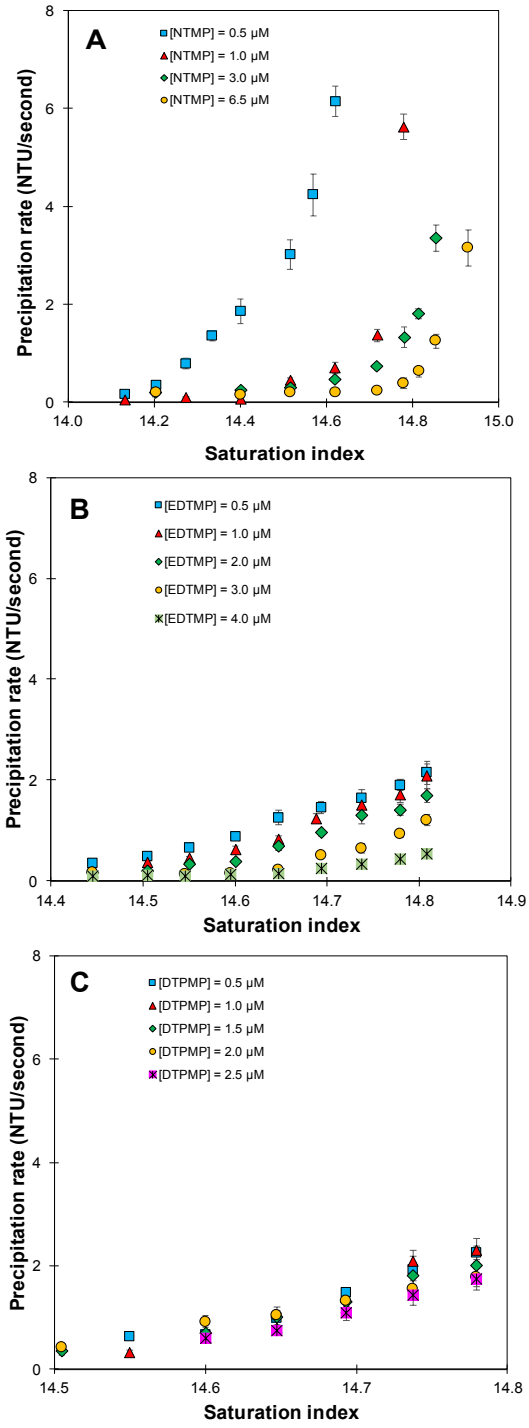

Figure 5 Impact of antiscalant dosage on rate of precipitation of hydroxyapatite in presence of (A): NTMP (saturation index = 14.1-14.9); (B): EDTMP (saturation index = 14.3-14.8) and (C): DTPMP (saturation index = 14.5-14.8). $[Ca^{2+}]$ = 10 mM; pH = 7.8; ionic strength = 100 mM; [TRIS buffer] = 20 mM.

386 **References**

1 Vörösmarty, C. J.; Green, P.; Salisbury, J.; Lammers, R. B. Global water resources: vulnerability from climate change and population growth. *Science* **2000**, 289 (5477), 284-288.

2 Trenberth, K. E. Changes in precipitation with climate change. *Climate Research* **2011**, 47, 123-138.

3 Seckin, G.; Yilmaz, T.; Sari, B.; Ersu, C. B. Groundwater hydrochemistry at the Mediterranean coastal plains—the case of Silifke, Turkey. *Desalination* **2010**, 253 (1), 164-169.

4 Giambastiani, B. M. S.; Colombani, N.; Mastrocicco, M.; Fidelibus, M. D. Characterization of the lowland coastal aquifer of Comacchio (Ferrara, Italy): hydrology, hydrochemistry and evolution of the system. *Journal of hydrology* **2013**, 501, 35-44.

5 Barlow, P. M.; Reichard, E. G. Saltwater intrusion in coastal regions of North America. *Hydrogeology Journal* **2010**, 18 (1), 247-260.

6 US Geological Survey. National Brackish Groundwater Assessment. USGS Water Availability and Use Science Program. https://water.usgs.gov/ogw/gwrp/brackishgw/brackish.html (Access on 2/5/2019)

7 Ahmed, M.; Shayya, W. H.; Hoey, D.; Al-Handaly, J. Brine disposal from reverse osmosis desalination plants in Oman and the United Arab Emirates. *Desalination* **2001**, 133 (2), 135-147.

8 Ruiz-García, A.; Ruiz-Saavedra, E.; Feo-García, J. Start-up of brackish water desalination for agricultural irrigation in the Canary Islands (Spain). *Desalination and Water Treatment* **2016**, 57 (48-49), 22734-22742.

9 Shannon, M. A.; Bohn, P. W.; Elimelech, M.; Georgiadis, J. G.; Marinas, B. J.; Mayes, A. M. Science and technology for water purification in the coming decades. *Nature* **2008**, 452 (7185), 301-310.

10 Côté, P.; Siverns, S.; Monti, S. Comparison of membrane-based solutions for water reclamation and desalination. *Desalination* **2005**, 182 (1-3), 251-257.

11 Werber, J. R.; Osuji, C. O.; Elimelech, M. Materials for next-generation desalination and water purification membranes. *Nature Reviews Materials* **2016**, 1, 16018.

12 Famiglietti, J.; S. The global groundwater crisis. *Nature Climate Change*. **2014**,4, 945-8.

13 El Saliby, I.; Okour, Y.; Shon, H. K.; Kandasamy, J.; Kim, I. S. Desalination plants in Australia, review and facts. *Desalination*. **2009**, 247, 1-4.

14 "Desalination (Brackish and Sea Water)." California Water Plan Update 2013. Retrieved November 28, 2018 from http://www.water.ca.gov/waterplan/docs/cwpu2013/Final/Vol3_Ch10_Desalination.pdf. (access on 2/5/2019)

15 Benecke, J.; Rozova, J.; Ernst, M. Anti-scale effects of select organic macromolecules on gypsum bulk and surface crystallization during reverse osmosis desalination. *Separation and Purification Technology* **2018**, 198, 68-78.

16 Shirazi, S.; Lin, C. J.; Chen, D. Inorganic fouling of pressure-driven membrane processes—a critical review. *Desalination* **2010**, 250 (1), 236-248.

17 Greenlee, L. F.; Lawler, D. F.; Freeman, B. D.; Marrot, B.; Moulin, P. Reverse osmosis desalination: water sources, technology, and today's challenges. *Water research* **2009**, 43 (9), 2317-2348.

18 Pramanik, B. K.; Gao, Y.; Fan, L.; Roddick, F. A.; Liu, Z. Antiscaling effect of polyaspartic acid and its derivative for RO membranes used for saline wastewater and brackish water desalination. *Desalination* **2017**, 404, 224-229.

19 Neveux, T.; Bretaud, M.; Chhim, N.; Shakourzadeh, K.; Rapenne, S. Pilot plant experiments and modeling of $CaCO_3$ growth inhibition by the use of antiscalant polymers in recirculating cooling circuits. *Desalination* **2016**, 397, 43-52.

20 Sheikhi, A.; Li, N.; van de Ven, T. G.; Kakkar, A. Macromolecule-based platforms for developing tailor-made formulations for scale inhibition. *Environmental Science: Water Research & Technology* **2016**, 2 (1), 71-84.

21 Ahmed, M.; Arakel, A.; Hoey, D.; Thumarukudy, M. R.; Goosen, M. F.; Al-Haddabi, M.; Al-Belushi, A. Feasibility of salt production from inland RO desalination plant reject brine: a case study. *Desalination* **2003**, 158 (1-3), 109-117.

22 Van der Bruggen, B.; Lejon, L.; Vandecasteele, C. Reuse, treatment, and discharge of the concentrate of pressure-driven membrane processes. *Environmental science & technology* **2003**, 37 (17), 3733-3738.

23 Santa Ana Watershed Project Authority Website; http://www.sawpa.org/brineline/what-is-it/ (access on 2/5/2019)

24 Owens-Bennett, E. L.; Trussell, B.; Monroy, I.; Trussell, R. Proposed solids formation recovery formula for the inland empire brine line; October 10, **2016**.

25 Benjamin, M. M.; Lawler, D. F.; Tobiason, J. E. Inland empire brine line expert panel; June 29-30, 2011.

26 Greenlee, L. F.; Testa, F.; Lawler, D. F.; Freeman, B. D.; Moulin, P. Effect of antiscalants on precipitation of an RO concentrate: metals precipitated and particle characteristics for several water compositions. *Water research* **2010**, 44 (8), 2672-2684.

27 Greenlee, L. F.; Testa, F.; Lawler, D. F.; Freeman, B. D.; Moulin, P. The effect of antiscalant addition on calcium carbonate precipitation for a simplified synthetic brackish water reverse osmosis concentrate. *Water research* **2010**, 44 (9), 2957-2969.

28 Hasson, D.; Drak, A.; Semiat, R. Induction times induced in an RO system by antiscalants delaying CaSO4 precipitation. *Desalination* **2003**, 157 (1-3), 193-207.

29 Darton, E. G.; Scale inhibition techniques used in membrane systems. *Desalination* **1997**, 113 (2), 227-229.

30 Austin, A. E.; Miller, J. F.; Vaughan, D.A.; Kircher, J.F. Chemical additives for calcium sulfate scale control. *Desalination* **1975**, 16 (3), 345-357.

31 Ketrane, R.; Saidani, B.; Gil, O.; Leleyter, L.; Baraud, F. Efficiency of five scale inhibitors on calcium carbonate precipitation from hard water: effect of temperature and concentration. *Desalination* **2009**, 249 (3), 1397-1404.

32 Abd-El-Khalek, D. E.; Abd-El-Nabey, B. A. Evaluation of sodium hexametaphosphate as scale and corrosion inhibitor in cooling water using electrochemical techniques. *Desalination* **2013**, 311, 227-233.

33 He, F.; Sirkar, K. K.; Gilron, J. Effects of antiscalants to mitigate membrane scaling by direct contact membrane distillation. *Journal of Membrane Science* **2009**, 345 (1), 53-58.

34 Nowack, B. The behavior of phosphonates in wastewater treatment plants of Switzerland. *Water research* **1998**, 32 (4), 1271-1279.

35 Kumar, P.S.; Ejerssa, W.W.; Wegener, C.C.; Korving, L.; Dugulan, A.I.; Temmink, H.; van Loosdrecht, M.C.; Witkamp, G.J. Understanding and improving the reusability of phosphate adsorbents for wastewater effluent polishing. *Water research* **2018**, 145, 365-374.

36 Sweeney, F. M.; Cooper, S.D. The development of a novel scale inhibitor for severe water chemistries. In SPE *International Symposium on Oilfield Chemistry* **1993**. Society of Petroleum Engineers.

37 Carter Jr, R. P.; Carroll, R. L.; Irani, R. R. Nitrilotri (methylenephosphonic acid), ethyliminodi-(methylenephosphonic acid), and diethylaminomethylphosphonic acid: acidity and calcium (II) and magnesium (II) complexing. *Inorganic Chemistry* **1967**, 6 (5), 939-942.

38 Pairat, R.; Sumeath, C.; Browning, F. H.; Fogler, H. S. Precipitation and dissolution of calcium− ATMP precipitates for the inhibition of scale formation in porous media. *Langmuir* **1997**, 13 (6), 1791-1798.

39 Knepper, T. P. Synthetic chelating agents and compounds exhibiting complexing properties in the aquatic environment. *TrAC Trends in Analytical Chemistry* **2003**, 22 (10), 708-724.

40 Yu, W.; Song, D.; Li, A.; Yang, H. Control of gypsum-dominated scaling in reverse osmosis system using carboxymethyl cellulose. *Journal of Membrane Science* **2019**, 577, 20-30.

41 Peters, E. M.; Chivavava, J.; Rodriguez-Pascual, M.; Lewis, A. E. Effect of a Phosphonate Antiscalant during Eutectic Freeze Crystallization of a Sodium Sulfate Aqueous Stream. *Industrial & Engineering Chemistry Research* **2016**, 55 (35), 9378-9386.

42 Rosenberg, Y. O.; Reznik, I. J.; Zmora-Nahum, S.; Ganor, J. The effect of pH on the formation of a gypsum scale in the presence of a phosphonate antiscalant. *Desalination* **2012**, *284*, 207-220.

43 Greenlee, L. F.; Testa, F.; Lawler, D. F.; Freeman, B. D.; Moulin, P. The effect of antiscalant addition on calcium carbonate precipitation for a simplified synthetic brackish water reverse osmosis concentrate. *Water research* **2010**, 44 (9), 2957-2969.

44 Shih, W. Y.; Albrecht, K.; Glater, J.; Cohen, Y. A dual-probe approach for evaluation of gypsum crystallization in response to antiscalant treatment. *Desalination* **2004**, 169 (3), 213-221.

45 Ruiz-García, A.; Feo-Garcia, J. Antiscalant cost and maximum water recovery in reverse osmosis for different inorganic composition of groundwater. *Desalination and Water Treatment* **2017**, 73, 46-53.

46 Duan, W.; Oota, H.; Sawada, K. Stability and structure of ethylenedinitrilopoly (methylphosphonate) complexes of the alkaline-earth metal ions in aqueous solution. *Journal of the Chemical Society, Dalton Transactions* **1999**, (17), 3075-3080.

47 Deluchat, V.; Bollinger, J. C.; Serpaud, B.; Caullet, C. Divalent cations speciation with three phosphonate ligands in the pH-range of natural waters. *Talanta* **1997**, 44 (5), 897-907.

48 Popov, K.; Rönkkömäki, H.; Lajunen, L.H. Critical evaluation of stability constants of phosphonic acids (IUPAC technical report). *Pure and applied chemistry* **2001**, 73 (10), 1641-1677.

49 Wang, F.; Davis, T. E.; Tarabara, V. V. Crystallization of calcium sulfate dihydrate in the presence of colloidal silica. *Industrial & Engineering Chemistry Research* **2010**, *49* (22), 11344-11350.

50 Söhnel, O.; Mullin, J.W. Interpretation of crystallization induction periods. *Journal of colloid and interface science* **1988**, 123 (1), 43-50.

51 Greenberg, G.; Hasson, D.; Semiat, R. Limits of RO recovery imposed by calcium phosphate precipitation. *Desalination* **2005**, 183 (1-3), 273-288.

52 Malki, M.; Abbas, V. Relationship between phosphate scales and silica fouling in wastewater RO membrane systems. *IDA Journal of Desalination and Water Reuse* **2013**, 5 (1), 15-24.

53 Ning, R. Y.; Troyer, T. L. Colloidal fouling of RO membranes following MF/UF in the reclamation of municipal wastewater. *Desalination* **2007**, 208 (1-3), 232-237.

54 Rathinam, K.; Oren, Y.; Petry, W.; Schwahn, D.; Kasher, R. Calcium phosphate scaling during wastewater desalination on oligoamide surfaces mimicking reverse osmosis and nanofiltration membranes. *Water research* **2018**, 128, 217-225.

55 Mitrouli, S. T.; Kostoglou, M.; Karabelas, A. J. Calcium carbonate scaling of desalination membranes: Assessment of scaling parameters from dead-end filtration experiments. *Journal of Membrane Science* **2016**, 510, 293-305.

56 Ray, J. R.; Wong, W.; Jun, Y. S. Antiscaling efficacy of $CaCO_3$ and $CaSO_4$ on polyethylene glycol (PEG)-modified reverse osmosis membranes in the presence of humic acid: interplay of membrane surface properties and water chemistry. *Physical Chemistry Chemical Physics* **2017**, 19(7), 5647-5657.

57 Hamdona, S. K.; Al Hadad, O. A. Influence of additives on the precipitation of gypsum in sodium chloride solutions. *Desalination* **2008**, 228 (1-3), 277-286.

58 Zhao, J.; Wang, M.; Lababidi, H.M.; Al-Adwani, H.; Gleason, K.K. A review of heterogeneous nucleation of calcium carbonate and control strategies for scale formation in multi-stage flash (MSF) desalination plants. *Desalination* **2018**, 442, 75-88.

59 Jurenka, R. A.; Chapman-Wilbert, M. Maricopa Ground Water Treatment Study: Water Treatment Technology Program Report No. 15. US Department of the Interior, Bureau of Reclamation, Denver, CO. **1996**.

60 Visual MINTEQ ver. 3.1 (released 2014) J. P. Gustafsson

61 Benjamin, M. M. Water chemistry. Waveland Press **2014**.

62 Menten, L.; Michaelis, M. I. Die kinetik der invertinwirkung. *Biochem Z* **1913**, *49*, 333-369.

63 American Public Health Association, American Water Works Association, Water Pollution Control Federation and Water Environment Federation, *Standard methods*

for the examination of water and wastewater **1915**. American Public Health Association.

64 Rahardianto, A.; McCool, B. C.; Cohen, Y. Reverse osmosis desalting of inland brackish water of high gypsum scaling propensity: kinetics and mitigation of membrane mineral scaling. *Environmental science & technology* **2008**, 42 (12), 4292-4297.

65 Zeiher, E. K.; Ho, B.; Williams, K. D. Novel antiscalant dosing control. *Desalination* **2003**, 157 (1-3), 209-216.

66 Klepetsanis, P. G.; Koutsoukos, P. G. Kinetics of calcium sulfate formation in aqueous media: effect of organophosphorus compounds. *Journal of crystal growth* **1998**, 193 (1-2), 156-163.

67 Oh, H. J.; Choung, Y. K.; Lee, S.; Choi, J. S.; Hwang, T. M.; Kim, J. H. Scale formation in reverse osmosis desalination: model development. *Desalination* **2009**, 238 (1-3), 333-346.

68 Li, F.; Zhang, B.; Wang, H.; Wu, Y. Ethylenediamine core, octamethylenephosphonic acid terminated, PAMAM dendrimer and its use as antiscalant. *U.S. Patent Application* **2014**, 13 (943), 672.

69 Janusz, W.; Skwarek, E. Study of sorption processes of strontium on the synthetic hydroxyapatite. *Adsorption* **2016**, 22 (4-6), 697-706.

70 Harding, I. S.; Rashid, N.; Hing, K. A. Surface charge and the effect of excess calcium ions on the hydroxyapatite surface. *Biomaterials* **2005**, 26 (34), 6818-6826.

71 He, S.; Oddo, J. E.; Tomson, M. B. The nucleation kinetics of calcium sulfate dihydrate in NaCl solutions up to 6 m and 90 C. *Journal of Colloid and Interface Science* **1994**, 162 (2), 297-303.

72 Lancia, A.; Musmarra, D.; Prisciandaro, M. Measuring induction period for calcium sulfate dihydrate precipitation. *AIChE Journal* **1999**, 45 (2), 390-397.

73 Mahmoud, M. H. H.; Rashad, M. M.; Ibrahim, I. A.; Abdel-Aal, E. A. Crystal modification of calcium sulfate dihydrate in the presence of some surface-active agents. *Journal of colloid and interface science* **2004**, 270 (1), 99-105.

74 Christoffersen, J.; Christoffersen, M.R. Kinetics of spiral growth of calcite crystals and determination of the absolute rate constant. *Journal of crystal growth* **1990**, 100 (1-2), 203-211.

75 Wu, W.; Nancollas, G. H. Determination of interfacial tension from crystallization and dissolution data: a comparison with other methods. *Advances in colloid and interface science* **1999**, 79 (2-3), 229-279.

76 Boistelle, R.; Lopez-Valero, I. Growth units and nucleation: the case of calcium phosphates. *Journal of crystal growth* **1990**, 102 (3), 609-617.

77 Becker, R. V.; Döring, W. Kinetic treatment of the formation of nuclei in over-saturated steam. *Ann Phys* **1935**, 5 (24), 719-752.

78 Frenkel, J. A. A general theory of heterophase fluctuations and pretransition phenomena. *The Journal of Chemical Physics* **1939**, 7 (7), 538-547.

79 Markov, I.V. Crystal Growth for Beginners: Fundamentals of Nucleation, Crystal Growth and Epitaxy. **2003**: World Scientific.

80 Myerson, A. S.; Jacovs, J.; Jacovs, J. Handbook of industrial crystallization **1993**. *Massachusetts: Butterworth-Heinemann.*

81 Opalko, F. J.; Adair, J. H.; Khan, S. R. Heterogeneous nucleation of calcium oxalate trihydrate in artificial urine by constant composition. *Journal of crystal growth* **1997**, 181 (4), 410-417.

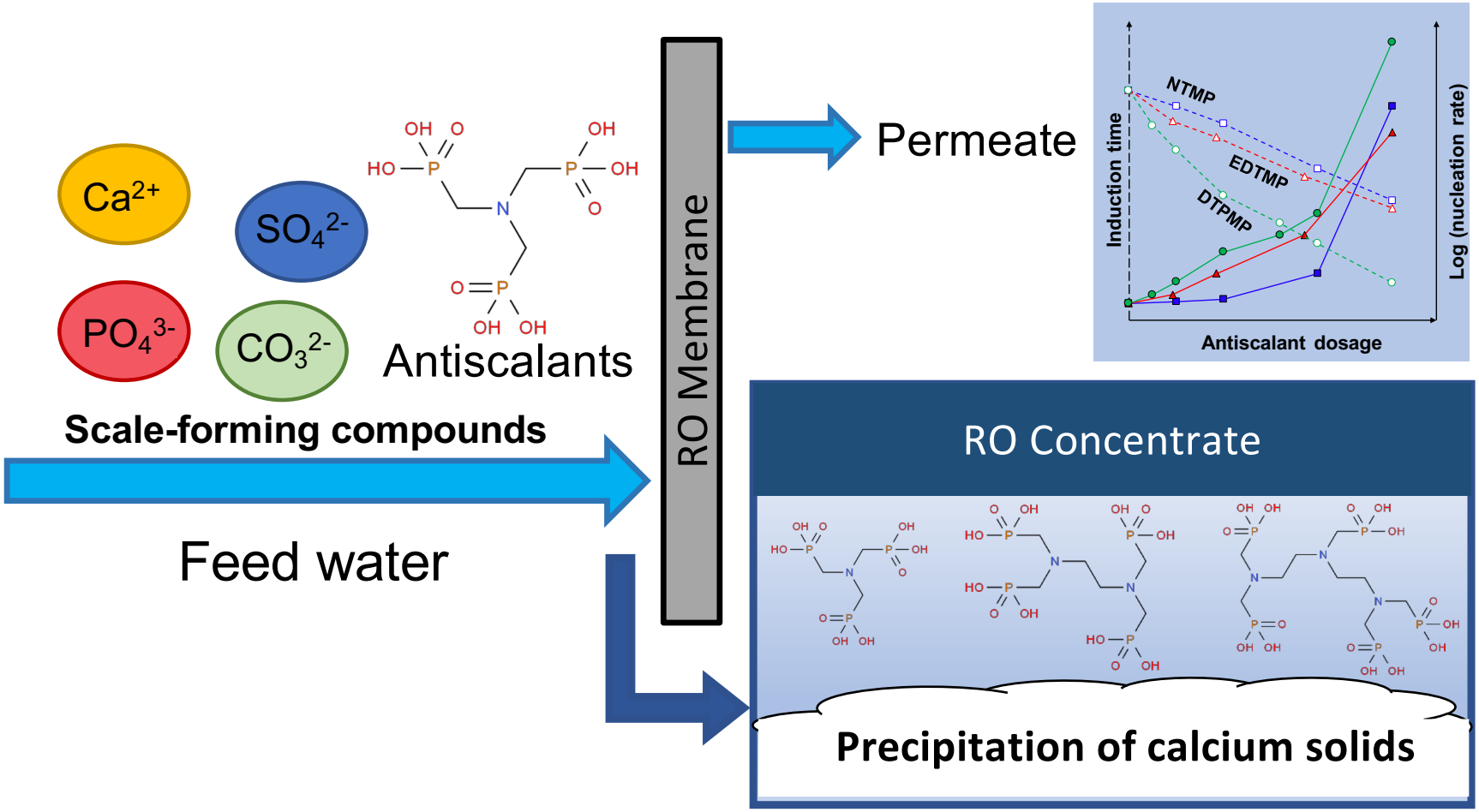
Ca2+
SO4 2-
PO4 3-
CO3 2-
Antiscalants
Scale-forming compounds
Feed water
RO Membrane
Permeate
NTMP
EDTMP
DTPMP
Induction time
Log (nucleation rate)
Antiscalant dosage
RO Concentrate
Precipitation of calcium solids